

Spatial correlation functions and the pairwise peculiar velocity dispersion of galaxies in the PSCz survey: implications for the galaxy biasing in cold dark matter models

Y.P. Jing

*Shanghai Astronomical Observatory, the Partner Group of MPI für Astrophysik,
Nandan Road 80, Shanghai 200030, China.*

and

*National Astronomical Observatories, Chinese Academy of Sciences,
Beijing 100012, China.*

ypjing@center.shao.ac.cn

Gerhard Börner

*Max-Planck-Institut für Astrophysik, Karl-Schwarzschild-Strasse 1,
85748 Garching, Germany*

grb@mpa-garching.mpg.de

and

Yasushi Suto

*Department of Physics and Research Center for the Early Universe (RESCEU)
School of Science, University of Tokyo, Tokyo 113-0033, Japan.*

suto@phys.s.u-tokyo.ac.jp

ABSTRACT

We report on the measurement of the two-point correlation function, and the pairwise peculiar velocity of galaxies in the IRAS PSCz survey. We compute these statistics first in redshift space, and then obtain the projected functions which have simple relations to the real-space correlation functions on the basis of the method developed earlier in analyzing the Las Campanas Redshift Survey (LCRS) by Jing, Mo, & Börner (1998). We find that the real space two-point correlation function can be fitted to a power law $\xi(r) = (r_0/r)^\gamma$ with $\gamma = 1.69$ and $r_0 = 3.70 h^{-1}\text{Mpc}$. The pairwise peculiar velocity dispersion $\sigma_{12}(r_p)$ is close to 400 km s^{-1} at $r_p = 3 h^{-1}\text{Mpc}$ and decreases to about 150 km s^{-1} at $r_p \approx$

$0.2 h^{-1}\text{Mpc}$. These values are significantly lower than those obtained from the LCRS.

In order to understand the implications of those measurements on the galaxy biasing, we construct mock samples for a low density spatially-flat cold dark matter model ($\Omega_0 = 0.3$, $\lambda_0 = 0.7$, $\Gamma = 0.2$, $\sigma_8 = 1$) using a set of high-resolution N-body simulations. Applying a stronger cluster-underweight biasing ($\propto M^{-0.25}$) than for the LCRS ($\propto M^{-0.08}$), we are able to reproduce these observational data, except for the strong decrease of the pairwise peculiar velocity at small separations. This is qualitatively ascribed to the different morphological mixture of galaxies in the two catalogues. Disk-dominated galaxy samples drawn from the theoretically constructed GIF catalog yield results rather similar to our mock samples with the simple cluster-underweight biasing.

Subject headings: galaxies: clustering - galaxies: distances and redshifts - large-scale structure of Universe - cosmology: theory - dark matter

1. Introduction

Large catalogs of galaxies which give the redshift and position of each source are the astronomical data sets from which quantitative information on the distribution and formation of the galaxies can be obtained. To read out this information requires the use of statistical tools, and to assess the importance of the results a quantitative comparison with theoretical models is obligatory.

In a recent series of papers (Jing, Mo, & Börner 1998; Jing & Börner 1998, 2001), various statistical quantities from the Las Campanas Redshift Survey (LCRS) have been determined including the two-point correlation function (2PCF), $\xi(r)$, the power spectrum, $P(k)$, the pairwise peculiar velocity dispersion (PVD), $\sigma_{12}(r)$, and the three-point correlation function (3PCF), $\zeta(r_{12}, r_{23}, r_{31})$. In addition, a detailed comparison between these observational results and the predictions of current cold dark matter (CDM) models has been carried out. Jing, Mo, & Börner (1998; JMB98 hereafter) have constructed 60 mock samples for each theoretical model from a large set of high-resolution N-body simulations. The observational selection effects can then be taken into account in the analyses of the theoretical models exactly as for the real observational data. JMB98 have demonstrated at length that such a procedure is essential for the proper comparison between models and observations.

JMB98 found that both the real-space 2PCF and the PVD can be measured reliably from the LCRS, and that the observed 2PCF for LCRS is significantly flatter than the mass 2PCF

in CDM models on scales $\lesssim 1 h^{-1}\text{Mpc}$. The observed PVD also turned out to be lower than that of the dark matter particles in these models. JMB98 introduced a cluster-underweight (CLW) biasing model to account for these discrepancies; CLW essentially assumes that the number of galaxies per unit dark matter mass in a massive halo of mass M decreases as $\propto M^{-\alpha}$. If $\alpha = 0.08$, the 2PCF and the PVD of the LCRS are well reproduced in a spatially-flat CDM model with $\Omega_0^{0.6}\sigma_8 \approx 0.4$, where Ω_0 is the density parameter of the model and σ_8 is the current rms linear density fluctuation within a sphere of radius $8 h^{-1}\text{Mpc}$. In fact, Carlberg et al. (1996) argue that this anti-bias is at the level observed for rich clusters of galaxies. We note here that this CLW has been applied also in recent analytic modeling of the galaxy distribution (Seljak 2000; Peacock & Smith 2000; Sheth et al. 2000).

In the present paper, we report on the measurements of the 2PCF and PVD of galaxies in another large redshift survey, the PSCz catalog, which has become publicly available recently (Saunders et al. 2000). Since galaxies in the PSCz survey are selected from the IRAS point source catalog, they are supposed to be preferentially dominated by late types in contrast to the LCRS galaxies. Thus the difference of those clustering statistics between LCRS and PSCz should be interpreted as an indication for the morphology-dependent biasing of galaxies.

The rest of the paper is organized as follows; we briefly describe the PSCz sample and the corresponding mock samples from simulations in §2. Then we present the results for the 2PCF of the PSCz in §3 which are compared with various model predictions in §4. Also shown there are the results for spiral *galaxies* predicted by the GIF simulation (Kauffmann et al. 1999a,b). Similarly we present in §5 and §6 the observational determination of PVD and its theoretical implications, respectively. Finally §7 contains a summary and further discussion.

2. The PSCz galaxy sample and our mock catalogs

The PSCz survey (Saunders et al. 2000) contains the redshifts for galaxies selected from the IRAS Point Source Catalog (PSC; Beichman et al. 1988). In total the PSCz catalogue contains 15411 galaxies with their flux at $60\mu\text{m}$ exceeding 0.6Jy across 84% of the entire sky. The high sky coverage and the uniformity make this publicly available survey an ideal data set for the statistical studies of galaxy clustering. Both those parts of the sky excluded from the survey and the selection function are well documented in Saunders et al. (2000). In the analysis below, we use a volume-limited sample of galaxies with redshifts less than 6000 km s^{-1} according to the flux at $60\mu\text{m}$ and also all the galaxies with redshifts between 6000 km s^{-1} and 20000 km s^{-1} , resulting in a final semi-volume limited sample of

9425 galaxies. The volume-limited sample within 6000 km s^{-1} should reduce the influence of the local supercluster on the statistics.

We construct a large set of mock samples, which have the same survey geometry, selection function and sampling rate as the real PSCz galaxies, from high-resolution cosmological N-body simulations. We emphasize that this is a very important aspect of our analysis in asserting the statistical significance of the results. We consider a spatially flat model with $(\Omega_0, \lambda_0, \Gamma, \sigma_8) = (0.3, 0.7, 0.2, 1.0)$, where λ_0 is the cosmological constant and $\Gamma = \Omega_0 h$ is the shape parameter of the CDM power spectrum (Bardeen et al. 1986). We use three different realizations for the model computed in a box size of $300 h^{-1}\text{Mpc}$ employing 256^3 (~ 17 million) particles (Jing & Suto 1998; Jing 1998). This set of parameters is now considered as the *standard* low-density CDM model. JMB98 have found that this model reproduces the 2PCF and the PVD of the LCRS reasonably well. An even better fit to the LCRS data was obtained for a model with $\Omega_0 = 0.2$. The changes for this model can be roughly seen by a simple scaling of the term $\sigma_8 \Omega_0^{0.6}$ which is proportional to the amplitude of the PVD.

The mock samples are generated in the same way as described in JMB98, using the selection function from the PSCz (Saunders et al. 2000). We construct 20 mock samples for each realization, and thus altogether 60 mock samples for the model. For each mock sample we apply the CLW bias (JMB98). The CLW model, by construction, gives less weight to the denser clusters than the dark matter model, and thus is especially appropriate for the PSCz which is supposed to be dominated by spiral galaxies preferentially avoiding the high-density cluster regions. To be more specific, we randomly select *galaxies* from the dark matter particles so that the number of galaxies per unit dark matter mass, N/M , becomes proportional to $M^{-\alpha}$ within a halo of mass M . We apply this anti-biasing scheme for all dark halos with $M > 7 \times 10^{11} h^{-1} M_\odot$. While the model with $\alpha = 0.08$ reproduces the 2PCF and the PVD for the LCRS data, we find (see below) that the PSCz data require $\alpha = 0.25$, indicating stronger anti-biasing than the optically selected galaxies.

In addition, we also construct 20 mock catalogs from the GIF data base (Kauffmann et al. 1999a,b) for comparison to our models and to the data. The GIF simulation adopts the same cosmological model, but with a slightly lower normalization of the linear power spectrum $\sigma_8 = 0.9$. The simulation box size is $141 h^{-1}\text{Mpc}$. The most important feature of the GIF data is that a semi-analytic galaxy formation model is implemented in contrast to our biasing scheme entirely on the basis of the gravitational clustering. We select “spiral galaxies” from the GIF mock samples according to their luminosity ratio B/T of the bulge and the total component. About 80% of those mock galaxies at the low end of B/T are retained for our analysis, taking into consideration the fact that the population of ellipticals is about 1/4 that of spirals in the local Universe.

It might be more appropriate to select “galaxies” according to their infrared fluxes for the present purpose. Fortunately, however, the clustering properties of IRAS galaxies do not sensitively depend on the infrared luminosity (Szapudi et al. 2000), nor do those of the GIF spirals seem to depend sensitively on the ratio B/T . Thus our results below are fairly robust with respect to small changes in the population of galaxies.

3. The two-point correlation functions for the PSCz galaxies

Quite a number of large galaxy catalogs, both two-dimensional (angular), and three-dimensional (redshift) catalogs, have been used to determine the 2PCF, and this statistic has now been established quite well. This statistic has produced constraints on theoretical models which are sensitive to the cosmological parameters, the initial power spectrum of the mass density fluctuations, and the biasing of specific galaxy types with respect to the dark matter, among others.

We use the following estimator to measure the 2PCF ξ_z in redshift space;

$$\xi_z(r_p, \pi) = \frac{4RR(r_p, \pi) \times DD(r_p, \pi)}{DR(r_p, \pi)^2} - 1, \quad (1)$$

where DD is the count of galaxy-galaxy pairs in the projected separation r_p and radial separation π bins, RR and DR are similar counts of pairs formed by two random points and by one galaxy and one random point, respectively.

We first display the redshift correlation function $\xi(s)$ in Figure 1, which is the circular average of $\xi_z(r_p, \pi)$ for a radius $s = \sqrt{r_p^2 + \pi^2}$. The error bars have been estimated by the bootstrap resampling technique using the formula of Mo, Jing, & Börner (1992). The resulting 2PCF is well fitted by $\xi(s) = (5 h^{-1}\text{Mpc}/s)^{1.2}$ for $s \leq 8 h^{-1}\text{Mpc}$, but falls faster than the power-law on larger separations in good agreement with previous results (Seaborne et al. 1999). Here we focus our discussion on the projected 2PCF and the PVD (Davis & Peebles 1983) because these two statistics have not been determined for the PSCz galaxies before as of the writing of this paper.

We estimate the projected 2PCF $w(r_p)$ from the integrated redshift 2PCF as

$$w(r_p) = \int_0^\infty \xi_z(r_p, \pi) d\pi = \sum_i \xi_z(r_p, \pi_i) \Delta\pi_i. \quad (2)$$

The summation runs from $\pi_1 = 0.5 h^{-1}\text{Mpc}$ to $\pi_{50} = 49.5 h^{-1}\text{Mpc}$ with $\Delta\pi_i = 1 h^{-1}\text{Mpc}$. JMB98 have shown that this method yields an unbiased estimate of $w(r_p)$ which is also

related to the real space 2PCF simply as

$$w(r_p) = \int_0^\infty \xi(\sqrt{r_p^2 + y^2}) dy. \quad (3)$$

Figure 2 plot the projected 2PCF for the PSCz with error bars estimated again with the bootstrap resampling technique. Our tests with the mock samples indicated that a standard scatter among different mock samples is actually comparable to these bootstrap errors. So we will use the bootstrap error for the observational estimates and the mock sample scatter for the comparison of the models with the observations.

We attempt a power-law fit of the real space 2PCF $\xi(r)$ to the observed $w(r_p)$ over $r_p \lesssim 20 h^{-1}\text{Mpc}$ yielding

$$\xi(r) = (r_0/r)^\gamma, \quad (4)$$

with

$$r_0 = 3.70 h^{-1}\text{Mpc}, \quad \gamma = 1.69. \quad (5)$$

The slopes are less than that for the LCRS ($\gamma = 1.82$), and the amplitudes are lower (JMB98). The error-bars are, however, substantially larger than for the LCRS, indicating that this catalog is somewhat noisier. The reason might be that the intrinsic clustering is weaker in this catalog and/or the volume surveyed by the catalog is smaller. There is some indication for a deviation from the power-law between $0.2 h^{-1}\text{Mpc}$ and $0.8 h^{-1}\text{Mpc}$, but it is not highly significant when considering the error-bars. The above best-fit parameters are in very good agreement with the result of the 1.2Jy sample, $\gamma = 1.66$ and $r_0 = 3.76 h^{-1}\text{Mpc}$ (Fisher et al. 1994a).

4. Comparison to the two-point correlation functions from the mock samples

Figure 3 compares the projected 2PCF $w(r_p)$ for the PSCz galaxies with those for the mock samples. The CLW bias model with $\alpha = 0.25$ reproduces the PSCz data quite well within the 1σ error (dotted lines); even the wiggly structure of the PSCz $w(r_p)$ below $0.8 h^{-1}\text{Mpc}$ is recovered. The value of α larger than for the optically selected galaxies (e.g., $\alpha = 0.08$ for the LCRS) is consistent with the observational density-morphology relation; spiral galaxies preferentially selected by the IRAS PSCz do not concentrate in dense cluster regions. Moreover it is interesting that our CLW bias model can account for this behavior in a quantitative manner, purely by an appropriate adjustment of the parameter α .

To follow up this point a bit more, we have also constructed mock catalogs from the GIF simulation data (Kauffmann et al. 1999a,b). From the simulated catalogue, we select those galaxies with $\Delta V_{bg} \equiv V_b - V_g \geq 1$, where V_b and V_g denote the V-band magnitudes of the

bulge and the whole galaxy. This encompasses about 80 percent of the galaxies in the GIF catalog. The resulting $w(r_p)$ again fits the observations quite well (Fig.3) for $r_p \gtrsim 1 h^{-1}\text{Mpc}$. While the amplitude of $w(r_p)$ for the GIF simulation is a bit larger than the PSCz data for $r_p \lesssim 1 h^{-1}\text{Mpc}$, it still lies close to the $+1\sigma$ error line of our CLW mock samples. So these semi-analytic models of galaxy formation which incorporate physical processes like star formation and supernova explosions in some global way have a similar effect of reducing the number of galaxies per unit dark matter mass as our simple bias prescription.

Figure 4 plots the 2PCFs in real space, $\xi(r)$, of the GIF mock samples with different selection criteria, all of which follow a power-law $\propto r^{-1.69}$ quite nicely. While selecting galaxies on the basis of their ΔV_{bg} reduces the 2PCF at $r \lesssim 1 h^{-1}\text{Mpc}$ compared with those for all galaxies, the two different criteria, $\Delta V_{bg} \geq 1$ and $\Delta V_{bg} \geq 1.5$, result in almost identical 2PCFs despite the fact that the latter case selects only 60% of the entire GIF galaxies.

In Figure 5 we display several 2PCFs for dark matter from our simulations, the CLW mock samples with $\alpha = 0.08$ and $\alpha = 0.25$, and the $\Delta V_{bg} \geq 1.0$ sample from the GIF data set. Clearly, as has been noted many times already (see e.g. JMB98), the dark matter particles from the full simulation produce a $\xi(r)$ which is too large and too steep for $r \lesssim 1 h^{-1}\text{Mpc}$. The CLW bias model with $\alpha = 0.08$ that fits the LCRS data well still predicts a much higher amplitude of $\xi(r)$ than the PSCz data which are in good agreement with $\alpha = 0.25$ model. The GIF spiral result lies between these two CLW bias models, and is closer to that of $\alpha = 0.25$ at $r \gtrsim 1 h^{-1}\text{Mpc}$. We also note that the result of all GIF galaxies is quite close to the CLW model with $\alpha = 0.08$.

In summary, we may conclude that one can reproduce the 2PCFs both for the PSCz galaxies and for the optically selected LCRS galaxies in a CDM model adopting a simple biasing prescription dependent on the type of galaxies in the sample, as long as Ω_0 is less than unity and the bias underweights galaxies in dense clusters. The semi-analytic GIF models may be a step on the way to provide a physical interpretation to the phenomenological CLW bias model.

5. The pairwise peculiar velocity dispersion for the PSCz galaxies

The Pairwise Velocity Dispersion (PVD) of galaxies is a well-defined statistical quantity which contains interesting information in principle on the cosmic matter distribution. The peculiar velocities of galaxies are determined by the action of the local gravitational fields, and thus they directly mirror the gravitational potentials caused by dark and luminous matter. The PVD is measured by modeling the distortions in the observed redshift-space

correlation function $\xi_z(r_p, \pi)$. The basic step in modeling is to write $\xi_z(r_p, \pi)$ as a convolution of the real-space 2PCF function $\xi(r)$ and the distribution function $f(v_{12})$ of the relative peculiar velocity v_{12} of galaxy pairs along the line of sight (Davis & Peebles 1983):

$$1 + \xi_z(r_p, \pi) = \int f(v_{12}) \left[1 + \xi(\sqrt{r_p^2 + (\pi - v_{12})^2}) \right] dv_{12}. \quad (6)$$

While the real-space 2PCF $\xi(r)$ can be directly estimated by inverting equation (3), we use the power-law fit (5) as in most previous work. For the velocity distribution function, we use the following exponential form which is supported from observations (Davis & Peebles 1983; Fisher et al. 1994b), theoretical models (Diaferio & Geller 1996; Sheth 1996; Seto & Yokoyama 1998), and direct simulations (Efstathiou et al. 1988; Magira, Jing, & Suto 1999):

$$f(v_{12}) = \frac{1}{\sqrt{2}\sigma_{12}} \exp\left(-\frac{\sqrt{2}}{\sigma_{12}}|v_{12} - \bar{v}_{12}|\right), \quad (7)$$

where \bar{v}_{12} is the mean infall velocity and σ_{12} is the dispersion of the 1-D pairwise peculiar velocities along the line of sight.

It is worth pointing out that the above modeling (eqs. [6] and [7]) is an approximation and the infall velocity \bar{v}_{12} is not known *a priori*, either. JMB98 demonstrated with the LCRS mock samples that the above procedure provides an accurate estimate of σ_{12} (within 20% accuracy) if \bar{v}_{12} is known separately. In other words, \bar{v}_{12} must be modeled carefully to allow a precise measurement of the dispersion $\sigma_{12}(r)$. In reality, however, \bar{v}_{12} in the real Universe is not fairly certain at the present. One might think that on small scales \bar{v}_{12} is negligible, but this is true only for very small scales indeed. The function \bar{v}_{12} rises quite sharply around $1 h^{-1}\text{Mpc}$ (Mo, Jing, & Börner 1997), reaching twice the Hubble velocity just beyond $1 h^{-1}\text{Mpc}$. Therefore the proper modeling of the infall velocity is crucial in an accurate measurement of the PVD $\sigma_{12}(r)$.

Here we adopt the approach of JMB98 to determine the PVD for the PSCz catalogue. Figure 6 displays the result of this modeling both for the case of a self-similar infall and for zero infall. The self-similar infall model has the same parameters as those used in JMB98, and is quite close to the mean pair velocity in CDM models with $\Omega_0^{0.6}\sigma_8 = 0.4$ for the relevant scales $r \lesssim 5 h^{-1}\text{Mpc}$. As emphasized in JMB98, only the use of some reasonable infall model (although the result is not very sensitive to the specific model used) gives a reliable reconstruction of the PVD, whereas the zero infall case does not even qualitatively reproduce the true value. We therefore consider the result of the self-similar infall as a reasonable estimate for the pairwise velocity dispersion of the PSCz galaxies.

The procedure yields much lower PVD for the PSCz than that for the LCRS: σ_{12} just reaches 300 km s^{-1} at $r_p = 1 h^{-1}\text{Mpc}$, whereas $\sigma_{12}(1 h^{-1}\text{Mpc}) = 570 \pm 80 \text{ km s}^{-1}$ for the

LCRS (JMB98). This is again qualitatively consistent with the fact that spirals have smaller random motions than the galaxies that reside in big clusters. Our result at $r_p \approx 1 h^{-1}\text{Mpc}$ is in good agreement with the value, 317 km s^{-1} , of Fisher et al. (1994b) for the 1.2Jy sample, although they did not show the scale-dependence of the PVD.

Very remarkable in Figure 6 is the decrease of the PVD for small separations. The bootstrap errors in Figure 6 are quite substantial. Again we find that the errors are much larger than for the LCRS. Nevertheless it seems significant that the PVD decreases down to about 200 km s^{-1} near $r_p = 0.2 h^{-1}\text{Mpc}$. In contrast the LCRS data did not exhibit such a fall-off, but rather the PVD stayed almost constant near 400 km s^{-1} . If we further take into account the observational error of redshifts (typically $\sim 120 \text{ km s}^{-1}$) and add it to the PVD measurement in quadrature, the real value becomes even smaller, $\sim 150 \text{ km s}^{-1}$ at $r_p = 0.2 h^{-1}\text{Mpc}$. The galaxy pairs in the PSCz catalog are seemingly “very cold”; they show very little random motion.

6. Comparison with the pairwise velocity dispersion from the mock samples

Figure 7 compares the PVD for the CLW and GIF mock samples with that for the PSCz galaxies. In all cases, the model predictions significantly exceed the estimate for the PSCz. Only around $r_p \approx 3 h^{-1}\text{Mpc}$ the disagreement is not serious, especially if the large error bars are taken into account. In fact, we may speculate that a CDM model with $\Omega_0 = 0.2$ may even produce quite a good fit to the data at larger r_p , since the amplitude of the PVD scales with $\sigma_8 \Omega_0^{0.6}$. Reducing the values of σ_{12} accordingly, brings agreement on scales larger than $3 h^{-1}\text{Mpc}$. There is, however, no way to reproduce the steep decrease towards small values ($\sim 150 \text{ km s}^{-1}$) at $r_p = 0.2 h^{-1}\text{Mpc}$ of the PSCz data.

This is really puzzling, because the LCRS galaxies do not show a signature like this. Even taking into account the large error bars at small scales, we have to concede a formal 3σ deviation from the model results. This is consistent with previous findings of Ostriker & Suto (1990), Schlegel et al. (1994) and Strauss, Ostriker, & Cen (1998), who found that the galaxies in the local neighborhood are very quiet and that the dispersion of galaxies in mild density regions are small compared with the CDM predictions (also see Peebles 1995; Nolthenius, Klypin, & Primack 1997; Baker, Davis, & Lin 2000). It may also be that the measurements as well as the models become somewhat unreliable on such small scales. The finite sizes of galaxies may also reduce the PVD somewhat. As shown in Suto & Jing (1997) this can amount to up to 10 percent, if $0.1 h^{-1}\text{Mpc}$ is taken as a fiducial size, but the effect can be more pronounced for large and interacting spiral galaxies.

Nonetheless our results present a new constraint on the well-defined PVD statistic that any successful galaxy formation theory should explain. At the moment, we may speculate that perhaps the spiral galaxies obey a very special velocity bias, or that the CDM models are way off in the description of small scale clustering as recently discussed in a different context (Spergel & Steinhardt 2000; Yoshida et al. 2000).

To separate clearly the effect of introducing the CLW bias and of constructing the mock catalogs, we present in Figures 8 and 9 the PVD from our full simulation for the CDM model and for the GIF simulation. The CDM models adopting the CLW bias with $\alpha = 0.08$ and $\alpha = 0.25$ have a significantly lower PVD than the dark matter. We can also see that the shape of the PVD is quite similar among the dark matter, the CLW, and the GIF samples, while the amplitude of the dark matter particle PVD is typically higher by a few 100 km s^{-1} . Again the GIF galaxies with $\Delta V_{bg} \geq 1.0$ or $\Delta V_{bg} \geq 1.5$ do not show any significant difference. The maximum in the PVD near $1 h^{-1}\text{Mpc}$ present in the full simulation and the GIF sample is much reduced by the construction of the mock catalogs, and also for the $\alpha = 0.25$ CLW models.

7. Discussion

We have analyzed the data set of the IRAS PSCz galaxies (Saunders et al. 2000), and computed the two-point correlation functions and the pairwise peculiar velocity dispersion for these galaxies. A power-law fit to the real-space 2PCF $\xi(r) = (r_0/r)^\gamma$ gives an exponent $\gamma = 1.69$, and a lower amplitude $r_0 = 3.70 h^{-1}\text{Mpc}$ than the value obtained for the Las Campanas Redshift Survey ($r_0 = 5 h^{-1}\text{Mpc}$). We show that these results can be very well reproduced from mock samples constructed for a high resolution CDM simulation with $\Omega_0 = 0.3$ and $\lambda_0 = 0.7$ if we apply a biasing model which strongly underweights galaxies in the dense cluster regions. While this CLW bias was originally introduced by JMB98 to fit the LCRS galaxies, the bias needed for the PSCz galaxies is much stronger. More specifically, we find that the number of galaxies per unit dark matter in massive halos of mass M should be proportional to $\propto M^{-\alpha}$ with $\alpha = 0.25$ for the PSCz, as compared to $\alpha = 0.08$ for the LCRS. The change of α from the LCRS to the PSCz is not unexpected, since IRAS galaxies tend to avoid high-density cluster regions. The biased mock catalogs fit the 2PCF of the PSCz galaxies extremely accurately. We also have selected samples from the GIF simulation and shown that appropriate data sets can be drawn from that numerical catalog which give similar 2PCF.

The pairwise peculiar velocity dispersion measured from the PSCz has a much lower value, about 300 km s^{-1} at $r_p = 1 h^{-1}\text{Mpc}$, than the LCRS result at that separation of

$570 \pm 80 \text{ km s}^{-1}$. All the simulation models which are consistent with the 2PCF of the PSCz predict significantly larger values for PVD, although the CLW bias reduces the PVD to within the 1σ limit of this value, at least near $3 h^{-1}\text{Mpc}$ (if $\Omega_0 = 0.2$). As discussed in the last section, the decrease of $\sigma_{12}(r_p)$ for $r_p \lesssim 1 h^{-1}\text{Mpc}$ for the PSCz data is significant, and cannot be reproduced by the models.

In conclusion, we find that the infrared selected galaxies in the PSCz have a lower and less steep two-point correlation function than the optically selected sample of the LCRS. The PVD of the PSCz galaxies is also lower, and has a different r_p dependence than the corresponding quantity measured from the LCRS. Spatially-flat CDM models with $\Omega_0 \sim 0.3$ can give a good fit to the data, except for the small-scale behavior of the PVD, if a strong cluster antibias is imposed. The infrared selected galaxies require a much stronger CLW bias than the optically selected ones.

Y.P.J. and G.B. are grateful for the hospitality extended toward them at the physics department of Tokyo university, and for support during their stay at RESCEU. Y.P.J. is supported in part by the One-Hundred-Talent Program, by NKBRSF(G19990754) and by NSFC(No.10043004), and G.B. by SFB375. We would like to thank G. Kauffmann for her advice on using the GIF data. The simulations were carried out on VPP/16R and VX/4R at the Astronomical Data Analysis Center of the National Astronomical Observatory, Japan.

REFERENCES

Baker, J. E., Davis, M., & Lin, H. 2000, ApJ, 536, 112

Bardeen, J., Bond, J.R., Kaiser, N., & Szalay, A.S., 1986, ApJ, 304, 15

Beichman, C.A. et al. 1988, IRAS Catalogs and Atlases, Vol.1: Explanatory Supplement (JPL)

Carlberg, R.,G., Yee, H.,K.,C., Ellingson, E., Abraham, R., Gravel, P., Morris, S., & Pritchett, C.J., 1996, ApJ, 462, 32

Davis, M., & Peebles, P.J.E., 1983, ApJ, 267, 465

Diaferio, A., & Geller, M.J. 1996, ApJ, 467, 19

Efstathiou, G., Frenk, C. S., White, S. D. M., & Davis, M. 1988, MNRAS, 235, 715

Magira, H., Jing, Y.P., & Suto, Y. 2000, 528,30

Fisher, K.B., Davis, M., Strauss, M.A., Yahil, A., & Huchra, J.P. 1994a, MNRAS, 267, 927

Fisher, K. B., Davis, M., Strauss, M. A., Yahil, A., & Huchra, J. 1994b, MNRAS, 266, 50

Jing, Y.P. 1998, ApJ, 503, L9

Jing, Y.P., Mo, H.J., & Börner, G. 1998, ApJ, 494, 1 (JMB98)

Jing, Y.P., & Börner, G. 1998, ApJ, 503, 37

Jing, Y.P., & Börner, G. 2001, MNRAS (in press); astro-ph/0101211

Jing, Y.P., & Suto, Y. 1998, ApJ, 494, L5

Kauffmann, G., Colberg, J.M., Diaferio, A., & White, S.D.M. 1999, MNRAS, 303, 188

Kauffmann, G., Colberg, J.M., Diaferio, A., & White, S.D.M. 1999, MNRAS, 307, 529

Mo, H.J., Jing, Y.P., & Börner, G., 1992, ApJ, 392, 452

Mo, H.J., Jing, Y.P., & Börner, G., 1993, MNRAS, 264, 825

Mo, H.J., Jing, Y.P., & Börner, G., 1997, MNRAS, 286, 979

Nolthenius, R., Klypin, A. A., & Primack, J. R. 1997, ApJ, 480, 43

Ostriker, J.P. & Suto, Y. 1990, ApJ, 348, 378

Peacock, J.A., & Smith, R.E. 2000, MNRAS, 318, 1144

Peebles, P. J. E. 1995, ApJ, 449, 52

Saunders, W. et al. 2000, MNRAS, 317, 55

Schlegel, D., Davis, M., Summers, F., & Holtzman, J. A. 1994, ApJ, 427, 527

Seaborne, M.D. et al. 1999, MNRAS, 309, 89

Seljak, U. 2000, MNRAS, 318, 203

Seto, N., & Yokoyama, J.I. 1998, ApJ, 492, 421

Sheth, R.K. 1996, MNRAS, 279, 1310

Sheth, R.K., Lam, H., Diaferio, A., & Scoccimarro, R. 2000, MNRAS, in press (astro-ph/0009167)

Spergel, D.N., & Steinhardt, P.J. 2000, Phys.Rev.Lett., 84, 3760

Strauss, M.A., & Willick, J. A. 1995, Phys. Rep., 261, 271

Strauss, M. A., Ostriker, J. P., & Cen, R. 1998, ApJ, 494, 20

Suto Y., & Jing Y.P. 1997, ApJS, 110, 167

Szapudi, I., Branchini, E., Frenk, C. S., Maddox, S., & Saunders, W. 2000, MNRAS, 318, L45

Yoshida, N., Springel, V., White, S.D.M., & Tormen, G. 2000, ApJ, 544, 87

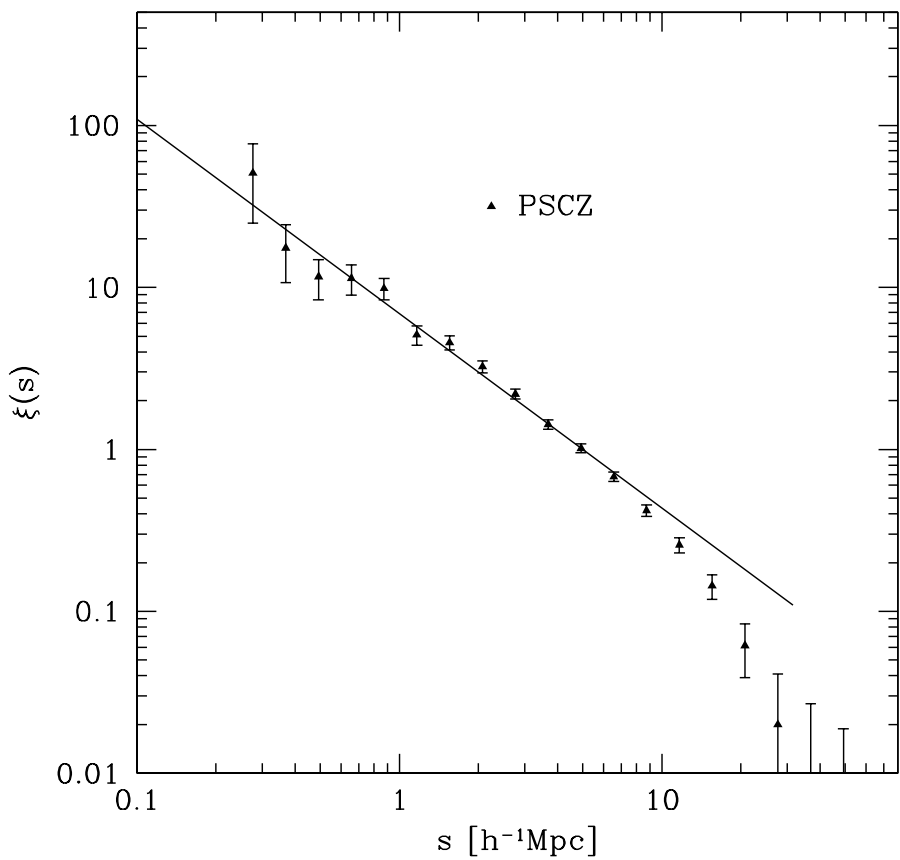


Fig. 1.— The redshift two-point correlation function measured from the PSCz catalog (filled triangles). The straight line is a power-law $(5 h^{-1}\text{Mpc}/s)^{1.2}$.

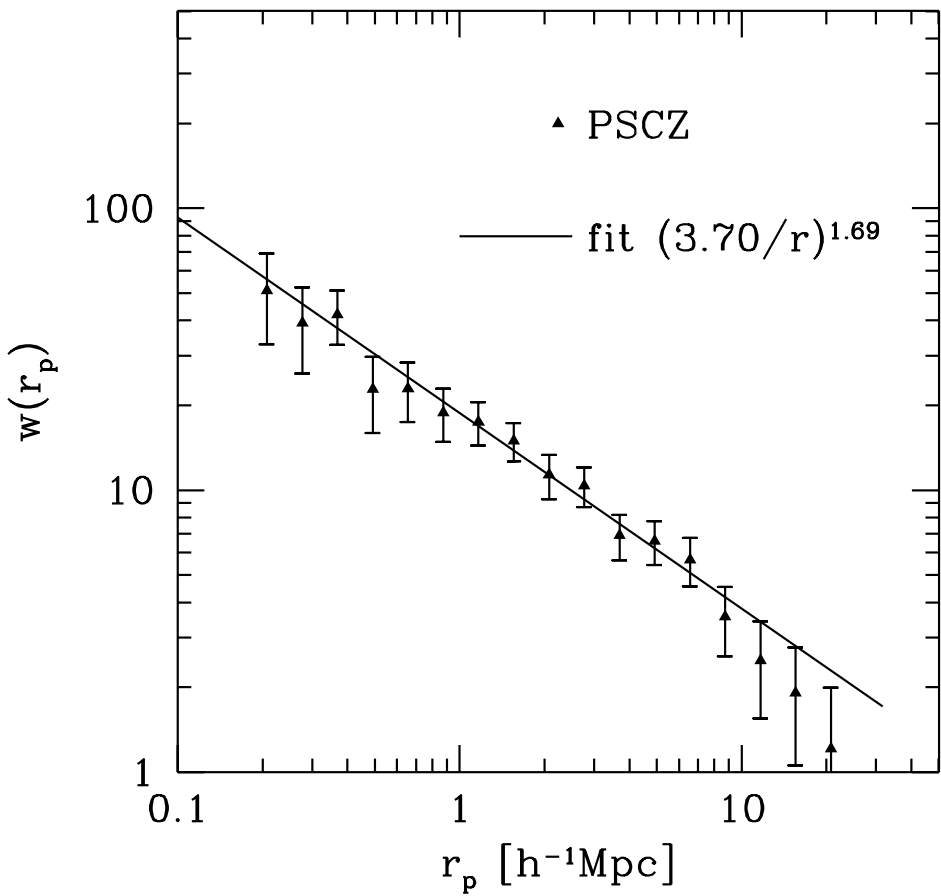


Fig. 2.— The projected two-point correlation function measured from the PSCz catalog (filled triangles). Error bars are 1σ deviations given by bootstrap resampling. The solid line is the best power-law fit.

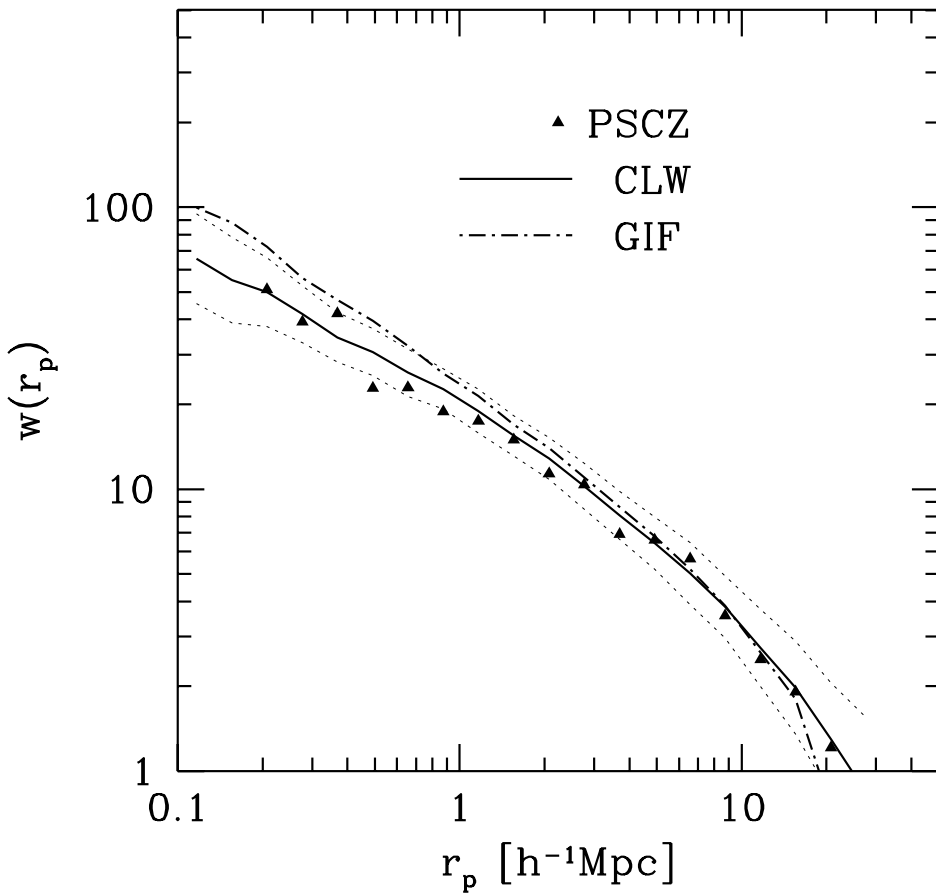


Fig. 3.— The predictions of CDM models vs the observation for the projected two-point correlation function. Triangles show the observational result. The mean value and the 1σ limits predicted by the cluster-weighted bias model are shown by the thick and thin lines respectively, and the mean value of the GIF simulation (without error bars) by the dot-dashed line.

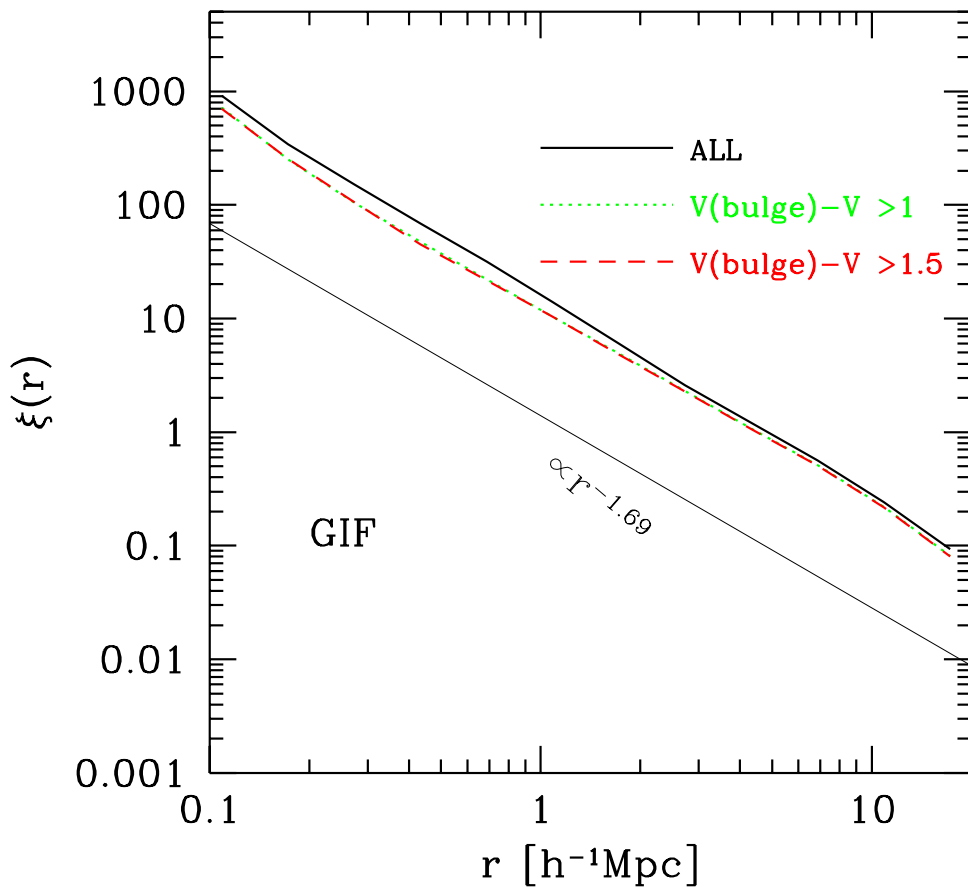


Fig. 4.— The real space two-point correlation functions of the galaxies selected in the GIF simulation based on the magnitude difference ΔV_{bg} between bulge and whole galaxy

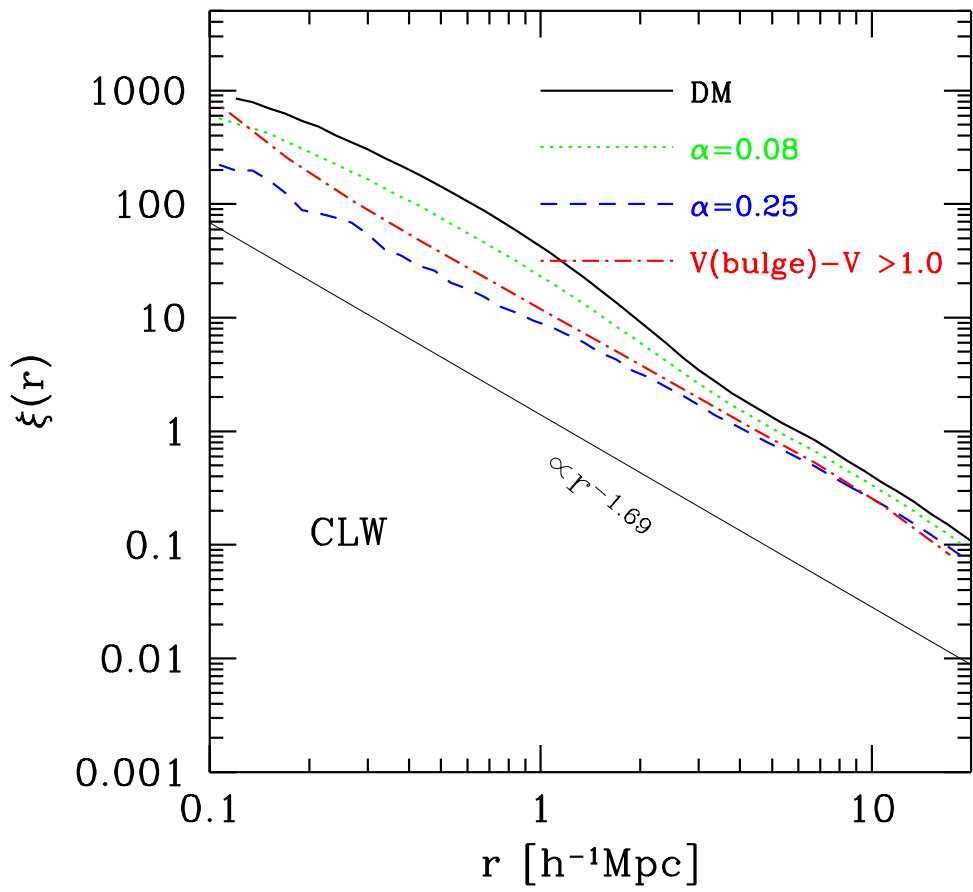


Fig. 5.— The real space two-point correlation functions of different bias tracers defined by the cluster-weighted model. For comparison, the result of the galaxies with $\Delta V_{bg} > 1$ in the GIF simulation are also plotted

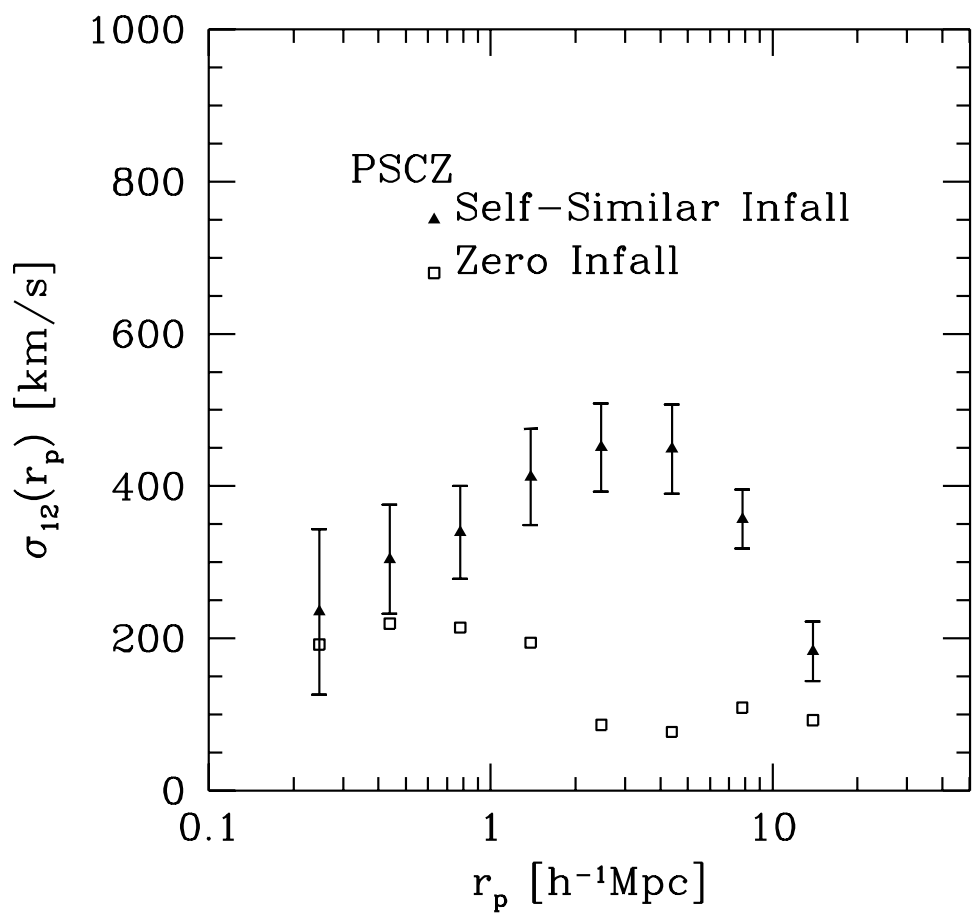


Fig. 6.— The pairwise velocity dispersion of the PSCz catalog determined for the self-similar infall (filled triangles) and for zero infall (open triangles).

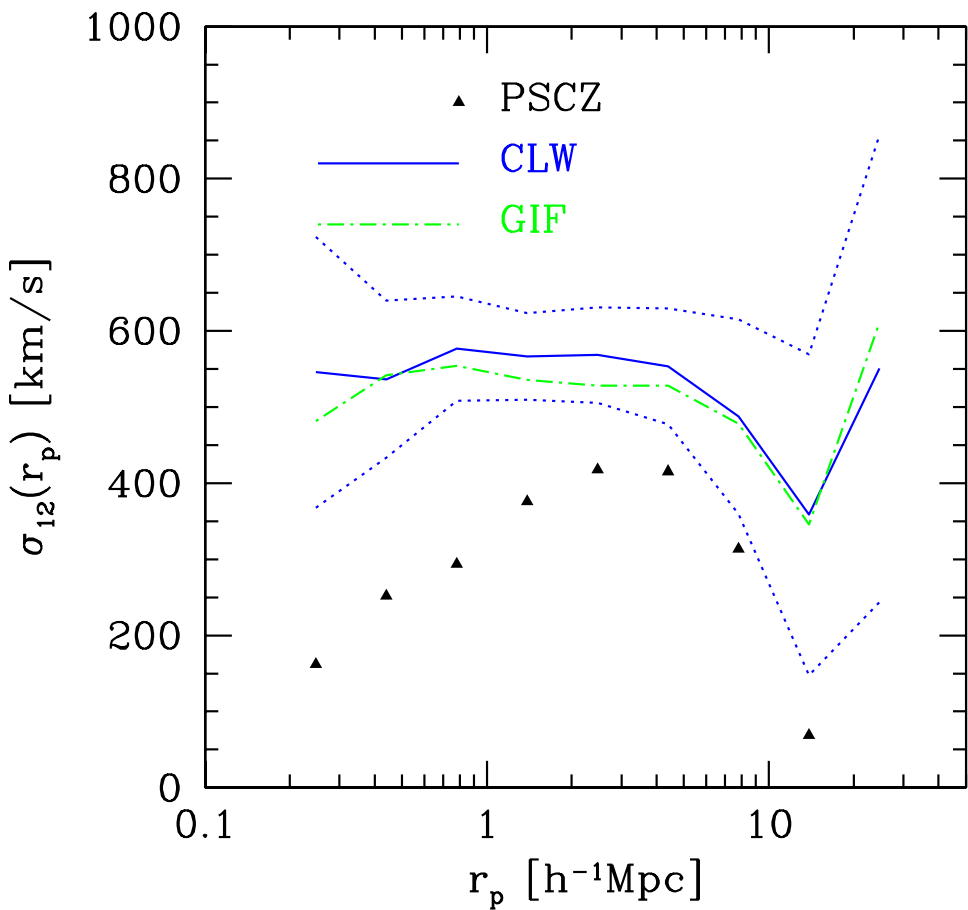


Fig. 7.— The predictions of CDM models vs the observation for the pairwise velocity dispersion. Triangles show the observational result which has been corrected for the observational error of redshifts in quadrature. The mean value and the 1σ limits predicted by the cluster-weighted bias model are shown by the thick and thin lines respectively, and the mean value of the GIF simulation (without error bars) by the dot-dashed line.

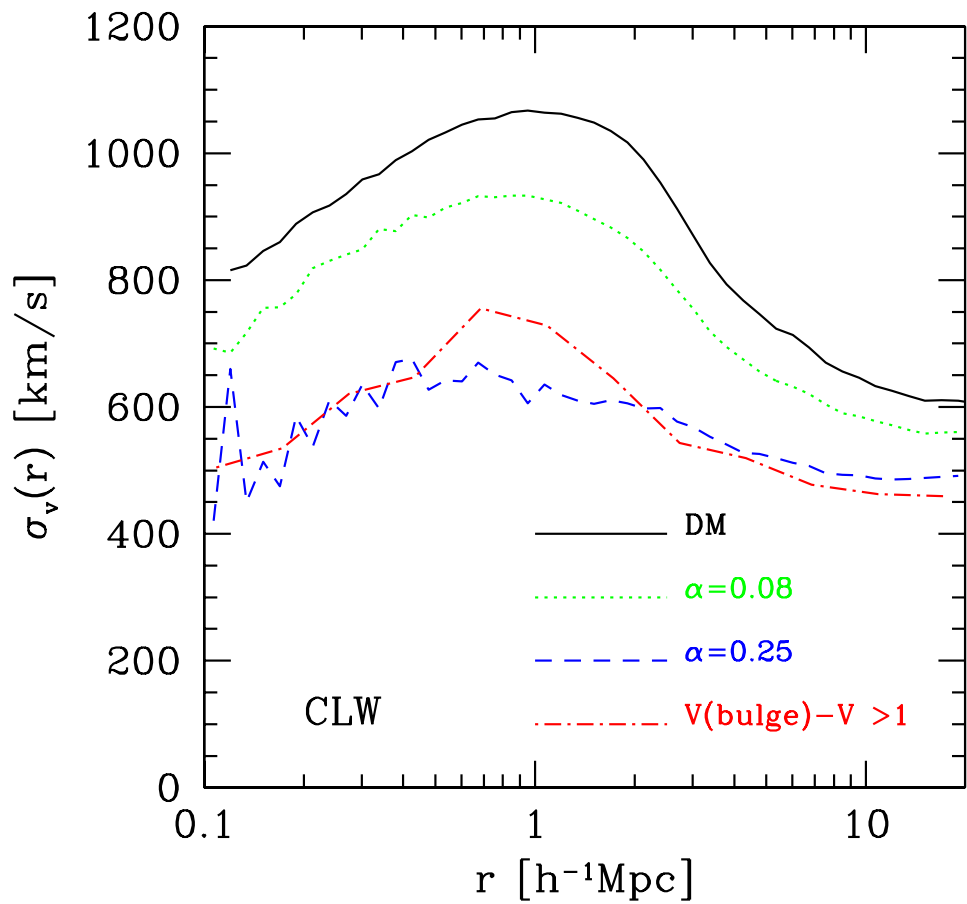


Fig. 8.— The pairwise velocity dispersion as determined from the 3-D velocity, of different bias tracers defined by the cluster-weighted model. For comparison, the result of the galaxies with $\Delta V_{bg} > 1$ in the GIF simulation are also plotted.

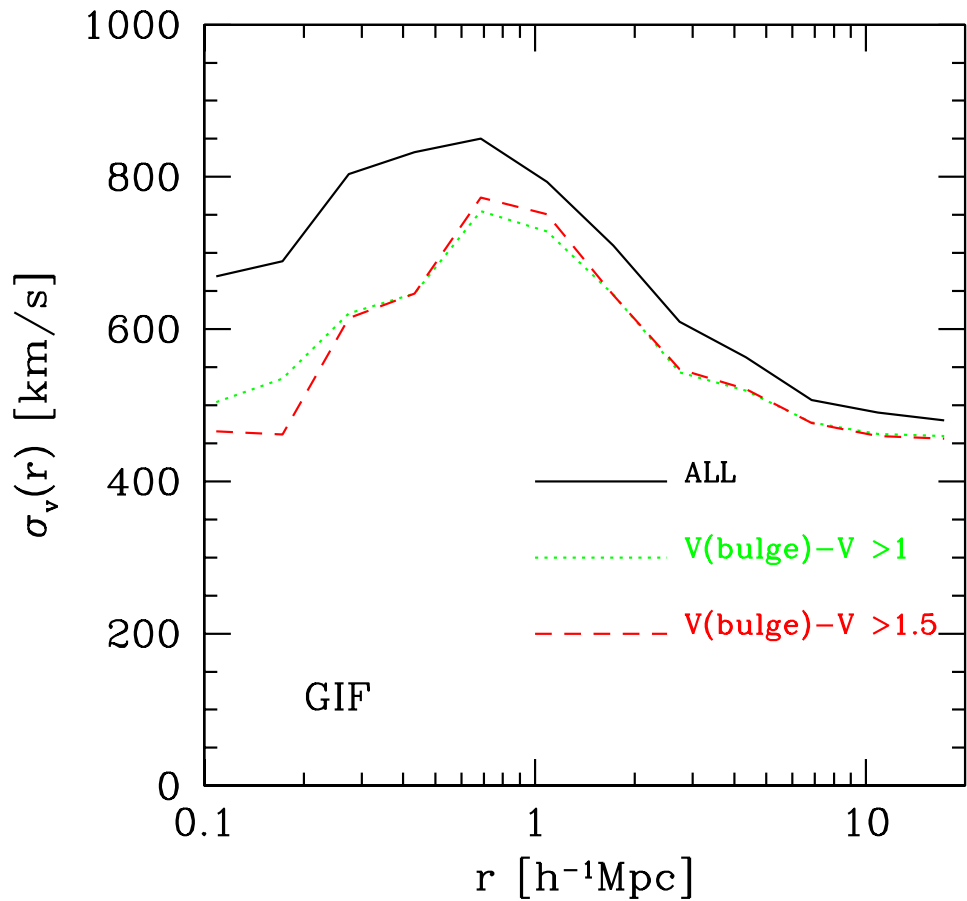


Fig. 9.— The pairwise velocity dispersion as determined from the 3-D velocity, of the galaxies selected in the GIF simulation based on the magnitude difference ΔV_{bg} between bulge and whole galaxy.